Phase transition of a non-Abelian quasiperiodic mosaic lattice model with *p*-wave superfluidity

Jincui Zhao,[1,2] Yujia Zhao,[1,2] Ji-Guo Wang,[3] Yueqing Li,[1,2,4] and Xiao-Dong Bai[5,*]

[1]*Department of Mathematics and Physics, Shijiazhuang TieDao University, Shijiazhuang 050043, China*
[2]*Institute of Applied Physics, Shijiazhuang TieDao University, Shijiazhuang 050043, China*
[3]*College of Physics and Electronic Science, Hubei Normal University, Huangshi 435002, China*
[4]*State Key Laboratory of Metastable Materials Science and Technology, Yanshan University, Qinhuangdao 066004, China*
[5]*College of Physics, Hebei Normal University, Shijiazhuang 050024, China*

(Received 4 October 2022; revised 14 June 2023; accepted 11 August 2023; published 22 August 2023)

It is now widely believed that *p*-wave superfluidity is the key to generate a novel critical phase in the non-Abelian Aubry-André-Harper model. However, we here establish that this belief is incorrect. In this work, we systemically investigate the phase transition of a non-Abelian quasiperiodic mosaic lattice model with *p*-wave superfluidity. The results show that the critical phase exists only in the quasiperiodic model, whereas in the mosaic model, despite the presence of *p*-wave superfluidity, the critical phase is absent, and mobility edge (ME) phases are generated instead. Furthermore, if the period of the mosaic modulation $\kappa \geqslant 3$, the results even show that regardless of the strength of the *p*-wave superfluidity, there are only extended and ME phases, but neither critical nor localized phases. This work clearly reveals the phase transition of a non-Abelian quasiperiodic mosaic lattice model with *p*-wave superfluidity, and it may be testified in near-term state-of-the-art experimental settings.

DOI: 10.1103/PhysRevB.108.054204

I. INTRODUCTION

Quantum phase transition is a fundamental physical phenomenon that has been extensively studied, and it has attracted the intense interest of both theorists and experimentalists in physics for decades [1–5]. One of the most reliable models to investigate such a phenomenon is the Aubry-André-Harper (AAH) model, which is easily implemented experimentally in photonic crystals [6,7] and ultracold atoms [8,9]. Up to now, it has been extensively used to understand the localization properties of many interesting systems, and has revealed a variety of transition properties between extended, critical, and localized phases [10–29].

Recent studies have shown that the introduction of *p*-wave superfluidity often significantly changes the dynamics, localizations, and topological transition properties of Hermitian and non-Hermitian AAH model systems [30–38]. For example, it is unveiled that the novel critical phase can exist in the AAH model once the *p*-wave superfluidity is added, while if the *p*-wave superfluidity is absent there are only two phases: extended and localized [38,39]. It seems to imply that the *p*-wave superfluidity is the most critical factor in generating the critical phase in the AAH model. Actually, these studies only explore the cases where the lattices are quasiperiodic models, so this belief is obviously controversial for understanding the nature of the critical phase. In order to address this issue, it is an essential task to elucidate the phase transition of some special AAH models, which are different from the quasiperiodic models but the *p*-wave superfluidity still exists.

Obviously, the mosaic disordered model is one of the best choice for such special AAH models. Many intriguing physical phenomena, such as mobility edges (MEs), topological phase transitions, localization phase transitions, and other quantum properties, have yielded pioneering achievements in the mosaic disordered models which are different from the quasiperiodic models [40–46]. Many of them have shown that the properties of these physical phenomena in the mosaic AAH models are usually different from that of quasiperiodic cases. For instance, there are no MEs in the standard AAH model, and it exhibits a phase transition from a completely extended phase to a completely localized phase with increasing the strength of the quasiperiodic potential. But, in the mosaic disordered AAH models one can obtain MEs in the energy spectra of the system [46]. Consequently, what is the phase transition property of the non-Abelian quasiperiodic mosaic model with *p*-wave superfluidity, and whether the introduction of mosaic modulation of a lattice can result in the absence of the critical phase in such a model, still remains unanswered and urgently needs to be explored.

Based on this motivation, in this work, we systemically explore the phase transition properties of such non-Abelian quasiperiodic mosaic lattice models with *p*-wave superfluidity. The results not only suggest that the critical phase exists only in the nonmosaic lattice model, but also show an intriguing phase diagram for a class of quasiperiodic mosaic lattice models. In the mosaic lattice model, in spite of the existence of *p*-wave superfluidity, the critical phase is absent, while the ME phases are generated instead. Furthermore, if the mosaic modulation $\kappa = 3$ and 4, there are even only extended and ME phases, and both critical and localized phases are absent. These results clearly reveal the phase transition of the non-Abelian quasiperiodic mosaic lattice model with *p*-wave superfluidity.

The remainder of this paper is organized as follows. In Sec. II, we introduce the one-dimensional (1D) non-Abelian

*xdbai@hebtu.edu.cn

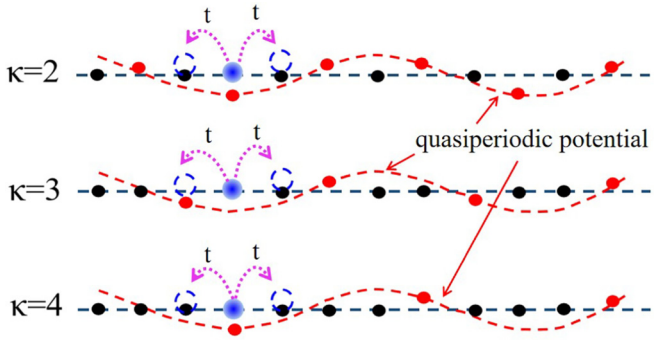

FIG. 1. Schematic illustration of the 1D quasiperiodic mosaic lattices with $\kappa = 2, 3, 4$. The red and black spheres represent the lattice sites whose potentials are quasiperiodic and zero, respectively, as shown by the corresponding red and navy blue dashed lines. The big blue sphere indicates a particle, and the nearest-neighbor constant hopping strength is t.

quasiperiodic mosaic lattice models with p-wave superfluidity. In Sec. III, we elaborate the calculation method for this issue in detail. In Sec. IV, we discuss the results of phase transition for some typical mosaic lattice models. Finally, we conclude in Sec. V.

II. MODEL

We consider a class of non-Abelian quasiperiodic mosaic models with p-wave superconducting pairing, which can be described as

$$\mathcal{H} = \sum_i [(\hat{\mathbf{c}}_{i+1}^\dagger \hat{T}_1 \hat{\mathbf{c}}_i + \text{H.c.}) + V_i \hat{\mathbf{c}}_i^\dagger \hat{T}_2 \hat{\mathbf{c}}_i], \tag{1}$$

with

$$V_i = \begin{cases} 2V\cos[2\pi(\omega i + \theta)], & i = m\kappa, \\ 0, & \text{otherwise}, \end{cases} \tag{2}$$

where $\hat{\mathbf{c}}_i = [\hat{c}_i^{(1)}, \hat{c}_i^{(2)}]^T$ represents a two-component field operator, and $\hat{c}_i^\dagger$ ($\hat{c}_i$) is the fermionic creation (annihilation) operator at the ith site; H.c. denotes the Hermitian conjugate; V, ω, θ denote the quasiperiodic potential amplitude, the irrational number, and the phase offset, respectively. κ is a fixed positive integer, and represents the period of the mosaic modulation. m is an integer running from 1 to N, i.e., $m = 1, 2, \ldots, N$. Then the system size will be $L = \kappa N$. It is obvious that this model reduces to the standard non-Abelian AAH model with p-wave superfluidity when $\kappa = 1$. If $\kappa \neq 1$ the system becomes a quasiperiodic mosaic model, and its schematic illustration is shown in Fig. 1 for $\kappa = 2, 3$, and 4, which has been similarly described in Ref. [46]. On the other hand, we here consider the simplest non-Abelian case with a two-component field operator and the SU(2) hopping matrices [47]:

$$\hat{T}_1 = t\hat{\sigma}_z - i\Delta\hat{\sigma}_y \tag{3}$$

and

$$\hat{T}_2 = \hat{\sigma}_z, \tag{4}$$

where $\hat{\sigma}_y$ and $\hat{\sigma}_z$ are the usual 2×2 Pauli matrices; t is the nearest-neighbor hopping coefficient and we set $t = 1$ for convenience; and Δ denotes the amplitude of p-wave superconducting pairing. If $\Delta = 0$, $\hat{T}_1$ and $\hat{T}_2$ could commute with each other, and the model will reduce to the standard AAH model for each component.

Note that in the absence of the disorder term (i.e., $V_i = 0$), the model of Eq. (1) describes a 1D topologically nontrivial insulator or a spinless p-wave superfluidity [48,49], while if $V_i \neq 0$, the model can describe the Majorana fermions in superconducting 1D systems or the 1D p-wave superconductor in the incommensurate lattices [30,31]. For these cases, the duality symmetry is held, and their phase transition properties have been extensively studied. In sharp contrast to these, the duality symmetry in the model of Eq. (1) is broken, and the related phase transition properties have not been investigated. Therefore, we aim to address the phase transition properties caused by symmetry breaking due to the introduction of mosaic modulation in this work. In experiments, the p-wave superfluidity amplitudes can be tuned by the mixture of spin-polarized fermions with a Bose-Einstein condensate [50,51], and the quasiperiodic mosaic lattices can be also easily implemented based on the result of Ref. [52].

III. METHOD

Following the similar derivation of Ref. [39], we assume that the two-component field operator $\hat{\mathbf{c}}_i = [\hat{c}_i^{(1)}, \hat{c}_i^{(2)}]^T$ and two SU(N) matrices are $\hat{T}_1$ and $\hat{T}_2$, then the wave function of the non-Abelian mosaic AAH model can be written as

$$|\psi\rangle = \sum_i \left[u_i \hat{c}_i^{(1)\dagger} + v_i \hat{c}_i^{(2)\dagger}\right]|0\rangle. \tag{5}$$

According to the Schrödinger equation $\mathcal{H}|\psi\rangle = \epsilon|\psi\rangle$, one can obtain

$$\begin{aligned} (u_{i+1} + u_{i-1}) + V_i u_i - \Delta(v_{i+1} - v_{i-1}) &= \epsilon u_i, \\ \Delta(u_{i+1} - u_{i-1}) - (v_{i+1} + v_{i-1}) - V_i v_i &= \epsilon v_i. \end{aligned} \tag{6}$$

Physically, for every particle-like solution (u_i, v_i) of the Schrödinger Eq. (6) with energy $E \geqslant 0$, there is always a hole-like solution (v_i^*, u_i^*) with energy $-E$. Following the typical choice in the literature, for the quasi-disorder potential V_i, we use an irrational number $\omega = [(\sqrt{5} - 1)/2]$, which is the inverse of the golden mean. It can be gradually approached by using the series of Fibonacci numbers F_n:

$$\omega = \lim_{n\to\infty} \frac{F_{n-1}}{F_n}, \tag{7}$$

where F_n is defined recursively by $F_{n+1} = F_{n-1} + F_n$, starting from $F_0 = F_1 = 1$. Thus, in numerical calculations we take the rational approximation:

$$\omega \simeq \omega_n = \frac{F_{n-1}}{F_n}. \tag{8}$$

To minimize the possible effect of the boundary, we take the periodic boundary condition.

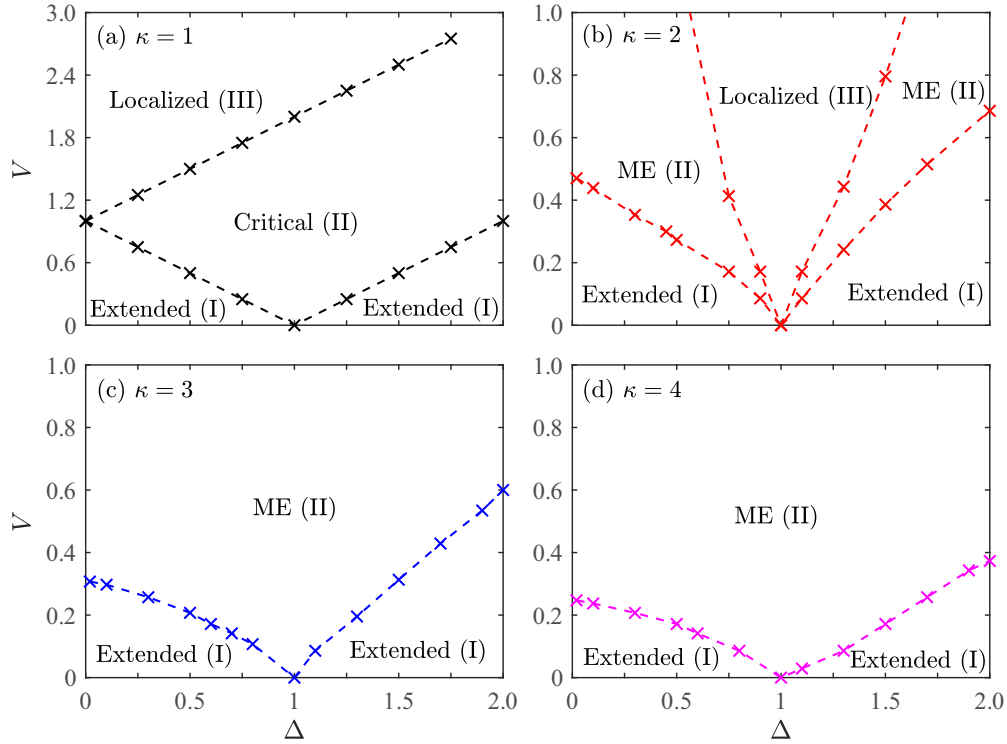

FIG. 2. Phase diagram of the non-Abelian quasi-disordered Fermi systems with p-wave order parameter Δ and disorder strength V for different periods of the mosaic modulation κ. (a) $\kappa = 1$, the system degenerates to the standard non-Abelian AAH model with p-wave superfluidity, and there are three different phases including extended, critical, and localized phases, as presented in Ref. [39]. (b) $\kappa = 2$, the system is described by the non-Abelian mosaic AAH model with p-wave superfluidity. Its result is obviously different from the case of $\kappa = 1$. The critical phase is absent, and there are extended, mobility edge, and localized phases. (c) $\kappa = 3$, the result is different from the cases of both $\kappa = 1$ and $\kappa = 2$; there are only extended and mobility edge phases. (d) $\kappa = 4$, the result is similar to the case of $\kappa = 3$. The crosses indicate the simulation results of the manuscript, and the black, red, blue, and magenta dashed lines indicate results from inter- and extrapolations.

Then, the model Hamiltonian $\mathcal{H}$ can be described by the following matrix:

$$\mathcal{H} = \begin{pmatrix} A_1 & B & 0 & \cdots & & 0 & C \\ B^\dagger & A_2 & B & 0 & \cdots & & 0 \\ 0 & B^\dagger & A_3 & B & 0 & \cdots & 0 \\ \vdots & \ddots & \ddots & \ddots & \ddots & \ddots & \vdots \\ 0 & \cdots & 0 & B^\dagger & A_{L-2} & B & 0 \\ 0 & & \cdots & 0 & B^\dagger & A_{L-1} & B \\ C^\dagger & & & \cdots & 0 & B^\dagger & A_L \end{pmatrix}, \quad (9)$$

where

$$A_i = 2V\cos(2\pi i\omega_n)\begin{pmatrix} 1 & 0 \\ 0 & -1 \end{pmatrix}, \quad (10)$$

$$B = \begin{pmatrix} 1 & -\Delta \\ \Delta & -1 \end{pmatrix}, \quad (11)$$

and

$$C = \begin{pmatrix} 1 & \Delta \\ -\Delta & -1 \end{pmatrix}. \quad (12)$$

Note that the C of Eq. (9) represents the periodic boundary condition, and it is utilized in all numerical simulations in this work. Now, the Schrödinger equation Eq. (6) can be solved by diagonalizing the matrix of Eq. (9), then one can obtain all the eigenvalues and the corresponding eigenvectors,

$$\psi = [u_{1,i_E}, v_{1,i_E}, \ldots, u_{i,i_E}, v_{i,i_E}, \ldots, u_{L,i_E}, v_{L,i_E}]^T, \quad (13)$$

where i is the number of the lattice site; $i_E = 1, 2, ..., 2L$ is the index of the i_Eth state of atoms; and u_{i,i_E} and v_{i,i_E} are the corresponding i_Eth wave function at the ith site.

Finally, in order to characterize the localization properties of this system, we introduce two useful quantities based on the inverse participation ratio (IPR). They are the mean inverse participation ratio (MIPR) and fractal dimension Γ. If the system has a pure energy spectrum, the extended, critical, and localized wave functions do not coexist, i.e., there are no MEs. The MIPR will be considered as a good choice to determine these phases, especially for the critical phase. It is given by

$$\text{MIPR} = \frac{1}{2L}\sum_{i_E=1}^{2L}\sum_{i=1}^{L}\left[u_{i,i_E}^4 + v_{i,i_E}^4\right], \quad (14)$$

where i_E is the index of energy levels. In the presence of disorder, for extended states, it is well known that the MIPR scales like $1/L$, while for localized states the MIPR tends to a finite value O(1). For critical states, the MIPR behaviors have other size dependence that is different from $1/L$ or O(1), but $1/L^\alpha$, where $0 < \alpha < 1$. By tuning the disorder strength, we

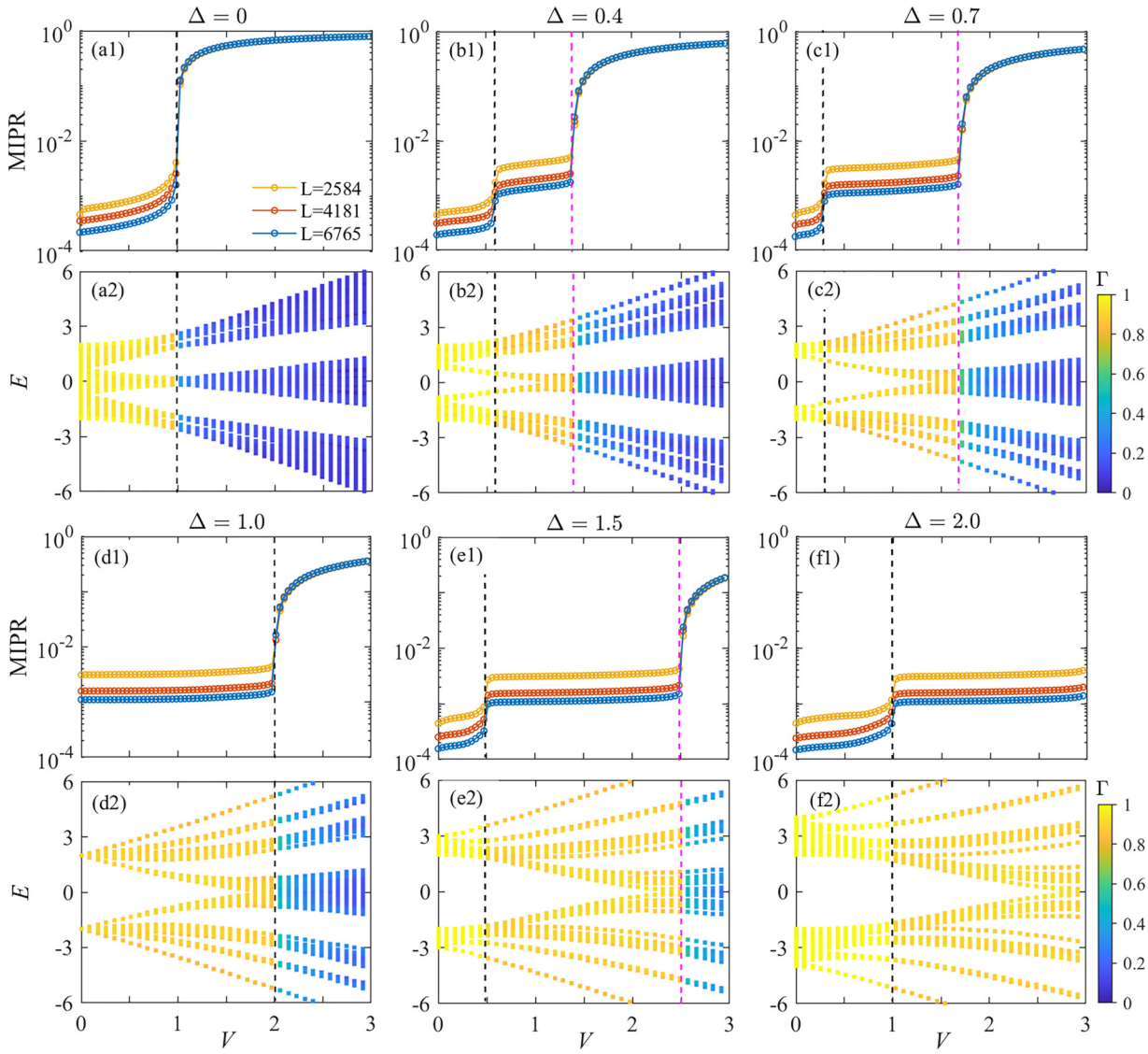

FIG. 3. The first and third rows represent the MIPR as a function of the quasi-disorder strength V for different Δ, where different lines denote $L = 2584$, 4181, and 6765, respectively. The second and fourth rows represent the fractal dimension Γ of eigenstates as a function of the corresponding eigenvalues and quasiperiodic potential strength V with $L = 6765$. The dashed lines show the sharp increase of the MIPR and Γ at phase boundaries. Here, we use $\kappa = 1$ in all cases.

anticipate a sharp change in MIPR, when the system transits from one phase to another.

However, if the system has MEs, which means the extended and localized states will coexist, the MIPR will not be able to distinguish this phase, because the localized states will significantly inhibit MIPR scaling down even if all the rest of the states are extended in the ME phase. Thus, to characterize the MEs we investigate the fractal dimension Γ of the wave function for each state, which is given by

$$\Gamma_{i_E} = -\frac{\ln\left(\sum_{i=1}^{L}\left[u_{i,i_E}^4 + v_{i,i_E}^4\right]\right)}{\ln L}. \tag{15}$$

In the presence of disorder, it is known that $\Gamma \to 1$ for extended states and $\Gamma \to 0$ for localized states as L increases. The fractal dimension Γ and its discussion are also adopted to describe the ME in Ref. [46]. Note that the Γ is insensitive to distinguishing the extended and critical phases because the difference between the wave functions of the extended and the critical states is generally small, which is demonstrated in Fig. 3. It can be seen that MIPR and Γ have their own advantages and disadvantages, thus we here take full advantage of them to systemically explore the phase transition of the non-Abelian quasiperiodic mosaic AAH model with p-wave superfluidity.

IV. RESULTS

A. Phase transitions

Based on the two quantities MIPR and Γ, we find that the phase transition properties of such a model are profoundly affected by both the existence of a nonzero Δ and the mosaic modulation κ. In contrast to the standard quasiperiodic AAH

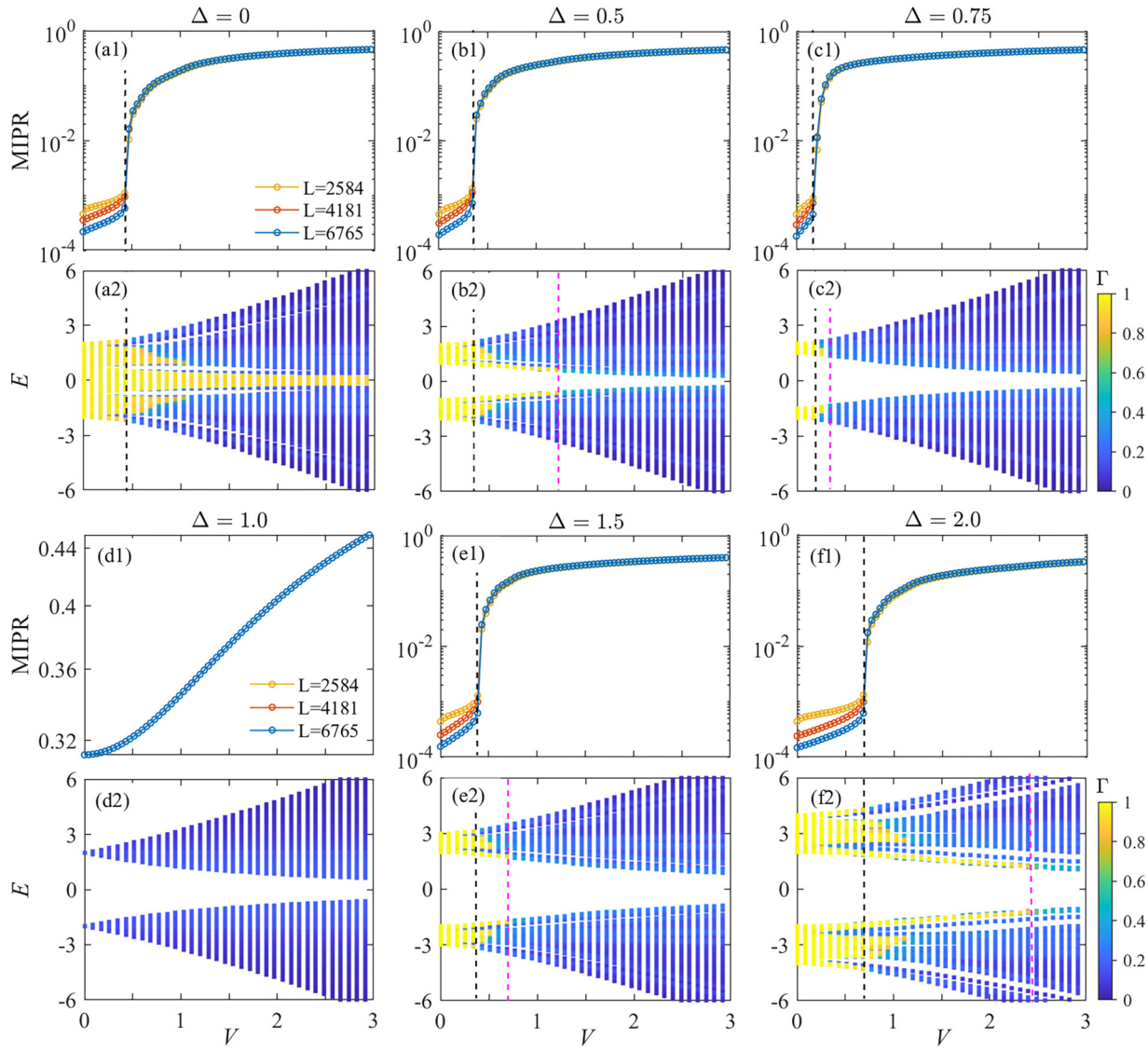

FIG. 4. The first and third rows represent the MIPR as a function of the quasi-disorder strength V for different Δ, where different lines denote $L = 2584$, 4181, and 6765, respectively. The second and fourth rows represent the fractal dimension Γ of eigenstates as a function of the corresponding eigenvalues and quasiperiodic potential strength V with $L = 6765$. The dashed lines show the sharp increase of the MIPR and Γ at phase boundaries. Here, we use $\kappa = 2$ in all cases.

model, the introduction of mosaic modulation of the lattice significantly changes the localization properties, and leads to some intriguing phase transition properties. The main results are summarized in the phase diagram shown in Fig. 2.

First, if $\kappa = 1$, the model reduces to the standard non-Abelian quasiperiodic AAH model with p-wave superfluidity, and its phase transition property has been systematically studied in Ref. [39]. Obviously, the results of Fig. 2(a) are consistent with those of the phase diagram in Ref. [39]. There are three phases: extended, localized, and critical, with the p-wave order parameter Δ and the disorder strength V. If $\kappa = 2$, this model becomes the non-Abelian quasiperiodic mosaic AAH model we focus on here. According to the results shown in Fig. 2(b), we can find that the introduction of mosaic modulation of lattice destroys the phase transition property of standard nonmosaic AAH model, and leads the critical phase to disappear despite the presence of p-wave superfluidity. Instead, three new phases are generated: extended, ME, and localized phases. If $\kappa = 3$ and $\kappa = 4$, the results are shown in Figs. 2(c) and 2(d). It can be seen that there are only extended and ME phases, and both critical and localized phases are absent.

These results demonstrate that the introduction of mosaic modulation of a lattice not only results in the absence of the critical phase in the non-Abelian AAH model, but also leads to some new phase diagrams as a function of both quasi-disorder and p-wave superfluidity for different classes of mosaic lattice models, which are greatly different from that of nonmosaic lattice models.

B. MIPR and Γ

In order to more clearly understand the phase diagram shown in Fig. 2, we plot Figs. 3–6, which report the evolution

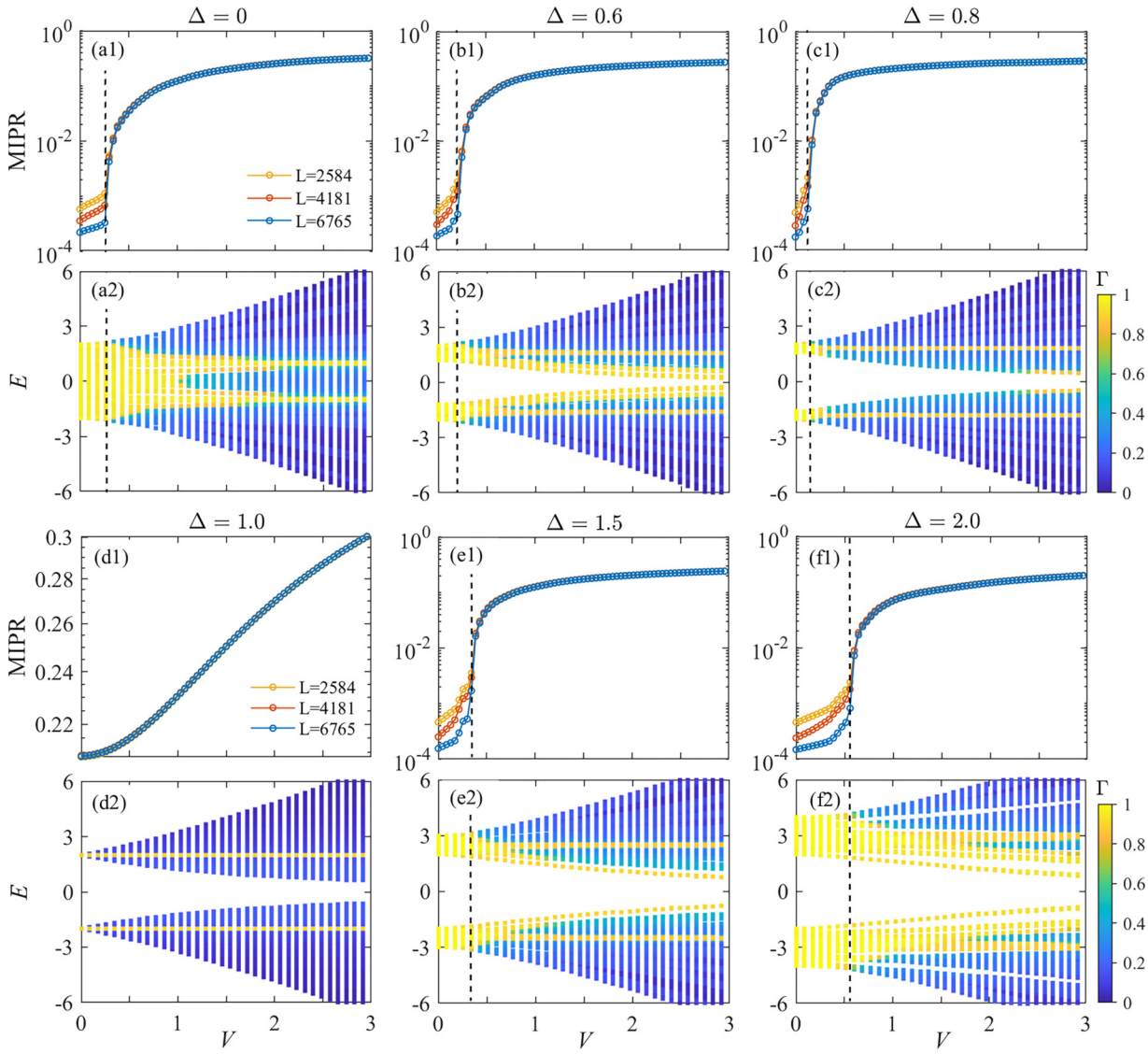

FIG. 5. The first and third rows represent the MIPR as a function of the quasi-disorder strength V for different Δ, where different lines denote $L = 2584$, 4181, and 6765, respectively. The second and fourth rows represent the fractal dimension Γ of eigenstates as a function of the corresponding eigenvalues and quasiperiodic potential strength V with $L = 6765$. The dashed lines show the sharp increase of the MIPR and Γ at phase boundaries. Here, we use $\kappa = 3$ in all cases.

of the MIPR and Γ for different parameters Δ and κ with V increasing.

1. The case of $\kappa = 1$

For $\kappa = 1$, the system is the standard non-Abelian quasiperiodic AAH model with p-wave superfluidity, and its result is reported in Fig. 3. If $\Delta = 0$, which means the system without p-wave superfluidity, we can find that there is one sharp increase in the MIPR, and one decrease in Γ correspondingly, which are marked by black dashed lines in Figs. 3(a1) and 3(a2). This suggests that there are two different phases. Further, the MIPR on the left of the dashed line scales like $1/L$, while the right of the dashed line is independent of L, as shown in Fig. 3(a1). Accordingly, the Γ on the left of the dashed line tends to 1, denoted by the yellow region, while the right of the dashed line tends to 0, denoted by the blue region, as shown in Fig. 3(a2). This meas the two phases are extended and localized phases, respectively.

If Δ increases to $\Delta = 0.4$ and $\Delta = 0.7$, we can find that the critical phases are generated, as shown in the middle area of black and magenta dashed lines in Figs. 3(b1)–3(c2). The behaviors of MIPR are significantly different from the extended and localized phases. However, there is only a small difference in Γ between the critical and extended phases, and if the color is not carefully tuned, this difference will not even be noticed. That is, the critical phase is sensitive to the MIPR but insensitive to Γ.

Similarly, if Δ increases to $\Delta = 1$, the extended phase disappears, and there are only critical and localized phases, as shown in Figs. 3(d1) and 3(d2). If Δ increases more, and $\Delta = 1.5$ and $\Delta = 2$, there are extended, critical, and localized phases again, as shown in Figs. 3(e1)–3(f2). These results discussed above correspond to Fig. 2(a).

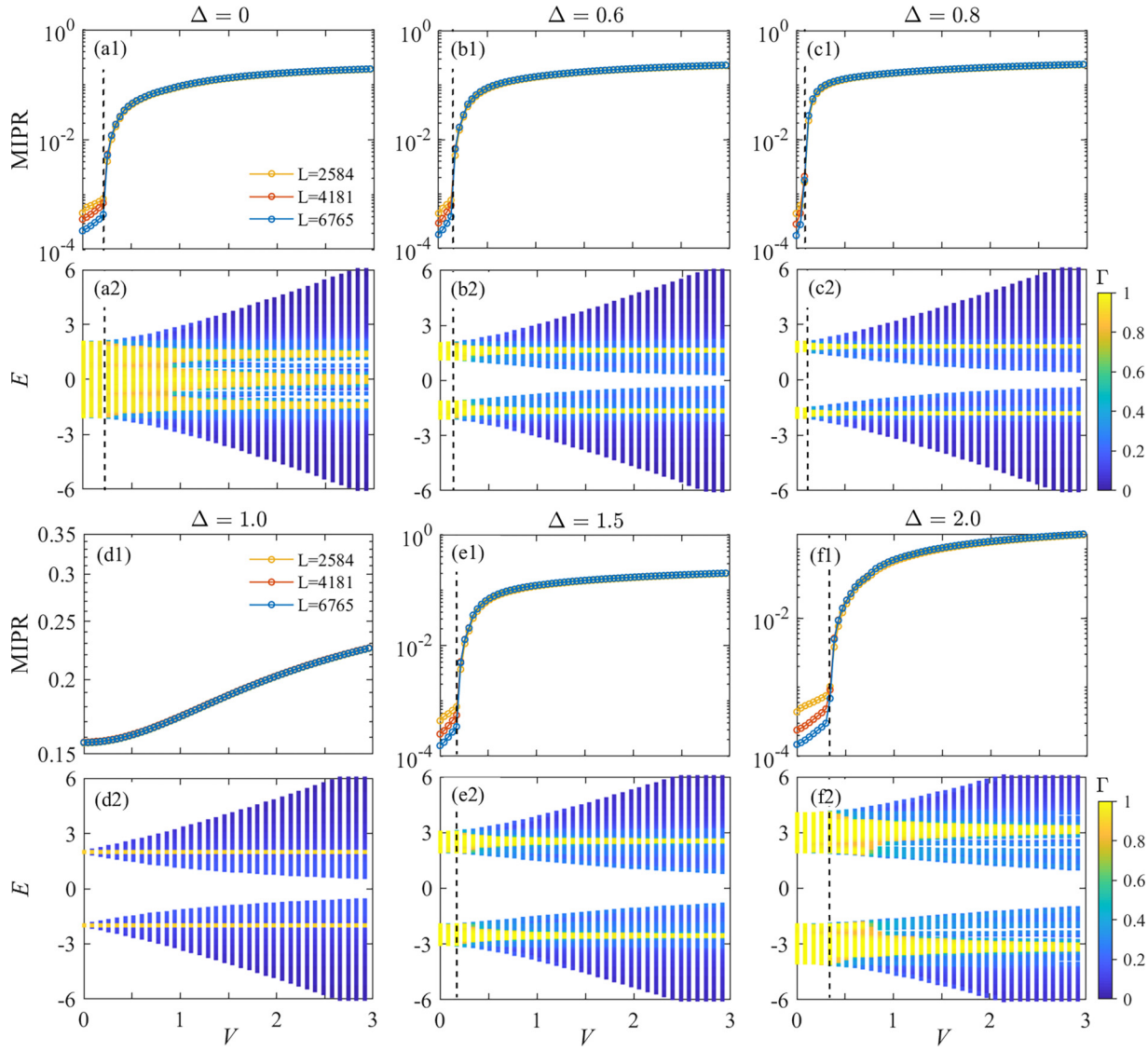

FIG. 6. The first and third rows represent the MIPR as a function of the quasi-disorder strength V for different Δ, where different lines denote $L = 2584$, 4181, and 6765, respectively. The second and fourth rows represent the fractal dimension Γ of eigenstates as a function of the corresponding eigenvalues and quasiperiodic potential strength V with $L = 6765$. The dashed lines show the sharp increase of the MIPR and Γ at phase boundaries. Here, we use $\kappa = 4$ in all cases.

2. The case of $\kappa = 2$

In this case, the system becomes the quasiperiodic mosaic AAH model with p-wave superfluidity, and its result is reported in Fig. 4. If $\Delta = 0$, the system has no p-wave superfluid, and there is one sharp increase in the MIPR, but decrease with mobility edge in Γ correspondingly, which are marked by black dashed lines in Figs. 4(a1) and 4(a2). The behaviors of both MIPR and Γ on the left of the dashed line are qualitatively similar to the case of $\kappa = 1$, which corresponds to the extended phase. On the right of the dashed line the results are clearly different from the case of $\kappa = 1$, and not all of Γ approach to 1. Some of Γ approach to 0, while the others approach to 1, despite that the MIPR is independent of L. That means it is not the localized phase, but the ME phase. Figure 4(a2) is very similar to Fig. 2(a) in Ref. [46], which indicates that the model in Ref. [46] is a special case of our model, i.e., $\Delta = 0$ and $\kappa = 2$.

If Δ increases to $\Delta = 0.5$ and $\Delta = 0.75$, we can find that there is still only one sharp increase in the MIPR and no significant change, as shown in Figs. 4(b1) and 4(c1). But there are two clear changes in Γ, and they are marked by black and magenta dashed lines, as shown in Figs. 4(b2) and 4(c2). Compared with the case of $\Delta = 0$, one of the most distinctive features is that this mobility edge does not exist all the time, but disappears before the magenta dashed line with V increasing. This means the ME phase stops at the magenta dashed line. On the right side of the magenta dashed lines, there are almost all localized states and no extended states. Thus, three regions correspond to extended, ME, and localized phases, respectively.

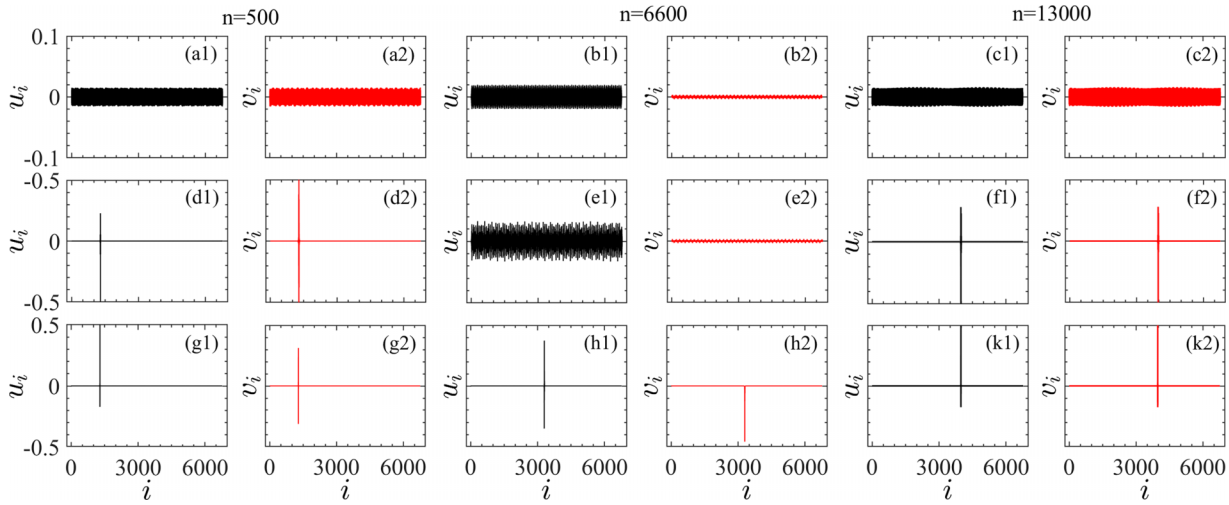

FIG. 7. The wave functions of different phases in Fig. 2(b) with $\Delta = 1.5$ for different V. u_i and v_i denote the wave functions of different components. The first, second, and third rows correspond to the extended, ME, and localized phases with $V = 0.1,\ 0.5$, and 1.5, respectively. The first two columns, middle two columns, and last two columns correspond to $n = 500,\ 6600$, and 13 000, respectively. Here, we use the system size $L = 6765$ for all cases.

As Δ increases again, if $\Delta = 1$ both the extended and ME phases degenerate and disappear, in which the MIPR is independent of L, and the Γ of all tends to 0. This means there is only the localized phase in the system, as shown in Figs. 4(d1) and 4(d2). If Δ increases more, i.e., $\Delta = 1.5$ and $\Delta = 2$, there are extended, ME, and localized phases again, as shown in Figs. 4(e1)–4(f2).

In addition, we can find that the critical strength of quasiperiodic potential marked by the black dashed line in Fig. 4(a) with $\Delta = 0$ is smaller than that of Fig. 3(a) in the standard quasiperiodic AAH model. This is because for the mosaic lattice the embedded zero potential sites have destroyed the quasiperiodic potential, and generate some uniform random disorder potentials.

The results discussed above correspond to Fig. 2(b). We can find that it is significantly different from the case of the nonmosaic lattice model ($\kappa = 1$), and there are extended, ME, and localized phases, while the critical phase is absent in the mosaic lattice model.

3. The cases of $\kappa = 3$ and $\kappa = 4$

In the case of $\kappa = 3$, if $\Delta = 0$ the results of both MIPR and Γ are qualitatively similar to the case of $\kappa = 2$, and there are two phases, extended and ME, as shown in Figs. 5(a1) and 5(a2). Note that Fig. 5(a2) is consistent with Fig. 2(b) in Ref. [46], which shows that our model becomes the model in Ref. [46] as the parameters have the values of $\Delta = 0$ and $\kappa = 3$. Different from the results of Figs. 4(b1)–4(c2), as Δ increases to $\Delta = 0.6$ and $\Delta = 0.8$, although the number of extended states decreases and that of localized states increases for Γ in the ME phase, there are still only the extended and ME phases, and the localized phase does not appear, as shown in Figs. 5(b1)–5(c2). As Δ increases again, if $\Delta = 1$ the extended and localized states always coexist in the system regardless of the value of V, which means there is only the ME phase, as shown in Figs. 5(d1) and 5(d2). If Δ increases more, and $\Delta = 1.5$ and $\Delta = 2$, the extended and ME phases appear again, as shown in Figs. 5(e1)–5(f2). These results correspond to Fig. 2(c).

In the case of $\kappa = 4$, the results are exactly similar to the case of $\kappa = 3$: if $\Delta = 1$ there is only the ME phase in the system, and there are extended and ME phases for other Δ, as shown in Fig. 6. These results correspond to Fig. 2(d).

It is worth pointing out that although these results are obtained based on ω being the inverse golden mean, we find that if ω is the inverse silver mean, the phase transition properties of such a model have not been changed in nature greatly.

C. The wave functions of different phases

In order to reconfirm the proposed phase diagram shown in Fig. 2, we further investigate the wave functions of different phases in Fig. 2(b) with $\Delta = 1.5$, and plot Fig. 7. In Fig. 7, we have chose the system size $L = 6765$, then the number of both eigenvalues and eigenstates is $2L = 13\,530$ because the system is two-component. u_i and v_i are the wave functions of different components. The first two columns, middle two columns, and last two columns correspond to $n = 500$, 6600, and 13 000, respectively, where n denotes the energy level of the eigenstate. The first, second, and third rows correspond to the extended, ME, and localized phases with $V = 0.1,\ 0.5$, and 1.5, respectively.

As we expected, if $V = 0.1$ the system corresponds to the extended phase, i.e., the wave functions of all states are extended, as shown in the first row of Fig. 7, which corresponds to Fig. 2(b) and the left of the black dash line in Figs. 4(e1) and 4(e2). In contrast, if $V = 0.5$ the system corresponds to the ME phase, where the extended and localized states coexist, i.e., the wave functions of low ($n = 500$) and high ($n = 13\,000$) energy states in the system are extended and others are localized, as shown in the second row of Fig. 7, which is verified by Fig. 2(b) and the middle of two dash lines in Figs. 4(e1) and 4(e2). Furthermore, if $V = 1.5$ the system corresponds to the localized phase, where the wave functions of all states are localized, as shown in the third row

of Fig. 7, which is consistent with Fig. 2(b) and the right of dash magenta line in Figs. 4(e1) and 4(e2).

V. CONCLUSION

In this work, we systemically explore the phase transition of non-Abelian quasiperiodic mosaic lattice models with p-wave superfluidity, aiming to address what are the phase transition properties of such mosaic models, and whether the introduction of mosaic modulation of a lattice can result in the absence of the critical phase in such a model. As a result, we find that the introduction of mosaic modulation in a lattice significantly changes the localization properties, and leads to some intriguing phase transition properties. The results show that in the mosaic lattice model, despite the presence of p-wave superfluidity, the critical phase is absent, and the mobility edge phases are generated instead. Furthermore, if the mosaic modulation $\kappa = 3$ and 4, there are even only extended and ME phases, and both critical and localized phases are absent. These results suggest that the introduction of mosaic modulation destroys the phase transition property of the standard nonmosaic AAH model. Finally, we give a clear phase diagram as a function of both quasi-disorder and p-wave superfluidity for different classes of mosaic lattice models. These results may be testified in near-term state-of-the-art experimental settings.

ACKNOWLEDGMENTS

This work is supported by the National Nature Science Foundation of China under Grants No. 11904242 and No. 12204325, and the open topic of State Key Laboratory of Metastable Materials Science and Technology of Yanshan University under Grant No. 202005.

[1] M. J. Hwang, R. Puebla, and M. B. Plenio, Phys. Rev. Lett. **115**, 180404 (2015).
[2] H. Shao, W. Guo, and A. W. Sandvik, Science **352**, 213 (2016).
[3] Z. Bi, E. Lake, and T. Senthil, Phys. Rev. Res. **2**, 023031 (2020).
[4] X.-D. Bai, J. Zhao, Y.-Y. Han, J.-C. Zhao, and J.-G. Wang, Phys. Rev. B **103**, 134203 (2021).
[5] W. Chen, S. Cheng, J. Lin, R. Asgari, and G. Xianlong, Phys. Rev. B **106**, 144208 (2022).
[6] Y. Lahini, R. Pugatch, F. Pozzi, M. Sorel, R. Morandotti, N. Davidson, and Y. Silberberg, Phys. Rev. Lett. **103**, 013901 (2009).
[7] Y. E. Kraus, Y. Lahini, Z. Ringel, M. Verbin, and O. Zilberberg, Phys. Rev. Lett. **109**, 106402 (2012).
[8] G. Roati, C. D'Errico, L. Fallani, M. Fattori, C. Fort, M. Zaccanti, G. Modugno, M. Modugno, and M. Inguscio, Nature (London) **453**, 895 (2008).
[9] G. Modugno, Rep. Prog. Phys. **73**, 102401 (2010).
[10] F. Evers and A. D. Mirlin, Rev. Mod. Phys. **80**, 1355 (2008).
[11] S. Aubry and G. André, Ann. Israel Phys. Soc **3**, 133 (1980).
[12] M. Kohmoto, L. P. Kadanoff, and C. Tang, Phys. Rev. Lett. **50**, 1870 (1983).
[13] S. Ostlund, R. Pandit, D. Rand, H. J. Schellnhuber, and E. D. Siggia, Phys. Rev. Lett. **50**, 1873 (1983).
[14] M. Kohmoto, Phys. Rev. Lett. **51**, 1198 (1983).
[15] D. J. Thouless, Phys. Rev. B **28**, 4272 (1983).
[16] H. Hiramoto and M. Kohmoto, Phys. Rev. B **40**, 8225 (1989).
[17] Y. Takada, K. Ino, and M. Yamanaka, Phys. Rev. E **70**, 066203 (2004).
[18] F. Liu, S. Ghosh, and Y. D. Chong, Phys. Rev. B **91**, 014108 (2015).
[19] S. Longhi, Phys. Rev. B **103**, 054203 (2021).
[20] Q.-B. Zeng, Y.-B. Yang, and Yong Xu, Phys. Rev. B **101**, 241104(R) (2020).
[21] Q.-B. Zeng, Y.-B. Yang, and Yong Xu, Phys. Rev. B **101**, 020201(R) (2020).
[22] P. He, Y.-G. Liu, J.-T. Wang, and S.-L. Zhu, Phys. Rev. A **105**, 023311 (2022).
[23] H. Li, Y.-Y. Wang, Y.-H. Shi, K. Huang, X. Song, G.-H. Liang, Z.-Y. Mei, B. Zhou, H. Zhang, J.-C. Zhang *et al.*, npj Quantum Inf. **9**, 40 (2023).
[24] A. M. Lacerda, J. Goold, and G. T. Landi, Phys. Rev. B **104**, 174203 (2021).
[25] W. Han and L. Zhou, Phys. Rev. B **105**, 054204 (2022).
[26] A. P. Acharya, A. Chakrabarty, D. K. Sahu, and S. Datta, Phys. Rev. B **105**, 014202 (2022).
[27] L. Z. Tang, G. Q. Zhang, L. F. Zhang, and D. W. Zhang, Phys. Rev. A **103**, 033325 (2021).
[28] L. J. Zhai, G. Y. Huang, and S. Yin, Phys. Rev. B **106**, 014204 (2022).
[29] Q. B. Zeng and R. Lü, Phys. Rev. B **105**, 245407 (2022).
[30] X. Cai, L. J. Lang, S. Chen, and Y. Wang, Phys. Rev. Lett. **110**, 176403 (2013).
[31] W. DeGottardi, D. Sen, and S. Vishveshwara, Phys. Rev. Lett. **110**, 146404 (2013).
[32] J. Fraxanet, U. Bhattacharya, T. Grass, M. Lewenstein, and A. Dauphin, Phys. Rev. B **106**, 024204 (2022).
[33] Q.-B. Zeng, S. Chen, and R. Lü, New J. Phys. **20**, 053012 (2018).
[34] M. Yahyavi, B. Hetényi, and B. Tanatar, Phys. Rev. B **100**, 064202 (2019).
[35] J. Fraxanet, U. Bhattacharya, T. Grass, D. Rakshit, M. Lewenstein, and A. Dauphin, Phys. Rev. Res. **3**, 013148 (2021).
[36] X. Tong, Y. M. Meng, X. Jiang, C. Lee, G. Dias de Moraes Neto, and G. Xianlong, Phys. Rev. B **103**, 104202 (2021).
[37] X. Cai, Phys. Rev. B **103**, 214202 (2021).
[38] T. Lv, T.-C. Yi, L. Li, G. Sun, and W.-L. You, Phys. Rev. A **105**, 013315 (2022).
[39] J. Wang, X.-J. Liu, G. Xianlong, and H. Hu, Phys. Rev. B **93**, 104504 (2016).
[40] D. Leykam, A. Andreanov, and S. Flach, Adv. Phys.: X **3**, 1473052 (2018).
[41] Y. Liu, Y. Wang, X.-J. Liu, Q. Zhou, and S. Chen, Phys. Rev. B **103**, 014203 (2021).
[42] D. Dwiputra and F. P. Zen, Phys. Rev. B **105**, L081110 (2022).
[43] B. P. Nguyen, D. K. Phung, and K. Kim, Phys. Rev. B **106**, 134204 (2022).
[44] Y. Liu, arXiv:2208.02762.
[45] Q.-B. Zeng and R. Lü, Phys. Rev. B **104**, 064203 (2021).

[46] Y. Wang, X. Xia, L. Zhang, H. Yao, S. Chen, J. You, Q. Zhou, and X. J. Liu, Phys. Rev. Lett. **125**, 196604 (2020).
[47] N. Goldman, A. Kubasiak, P. Gaspard, and M. Lewenstein, Phys. Rev. A **79**, 023624 (2009).
[48] M. Z. Hasan and C. L. Kane, Rev. Mod. Phys. **82**, 3045 (2010).
[49] X.-L. Qi and S.-C. Zhang, Rev. Mod. Phys. **83**, 1057 (2011).
[50] J. J. Kinnunen, Z. Wu, and G. M. Bruun, Phys. Rev. Lett. **121**, 253402 (2018).
[51] B. Liu, X. Li, R. G. Hulet, and W. V. Liu, Phys. Rev. A **94**, 031602(R) (2016).
[52] J. Gao, I. M. Khaymovich, X. W. Wang, Z. S. Xu, A. Iovan, G. Krishna, A. V. Balatsky, V. Zwiller, and A. W. Elshaari, arXiv:2306.10829.